Selectivity Filter Residues Contribute Unequally to Pore Stabilization in Voltage-Gated Sodium Channels†

Karlheinz Hilber,‡,|| Walter Sandtner,‡,|| Touran Zarrabi,‡ Eva Zebedin,‡ Oliver Kudlacek,‡ Harry A. Fozzard,§ and Hannes Todt*,‡

Center of Biomolecular Medicine and Pharmacology, Medical University of Vienna, Vienna, Austria, and Cardiac Electrophysiology Laboratories, The University of Chicago, Chicago, Illinois 60637

Received June 22, 2005; Revised Manuscript Received August 23, 2005

ABSTRACT: Mutations in the putative selectivity filter region of the voltage-gated Na^+ channel, the so-called DEKA-motif, not only affect selectivity but also alter the channel's gating properties, suggesting functional coupling between permeation and gating. We have previously reported that charge-altering mutations at position 1237 in the P-loop of domain III (position K of the DEKA-motif in the adult rat skeletal muscle Na^+ channel, $rNa_v1.4$) dramatically enhanced entry to an inactivated state from which the channels recovered with a very slow time constant on the order of ~100 s (Todt, H., Dudley, S. C. J., Kyle, J. W., French, R. J., and Fozzard, H. A. (1999) *Biophys. J. 76*, 1335−1345). This state, termed "ultra-slow inactivation", may reflect a complex molecular rearrangement of the channel's pore region that involves both the extracellular and the cytoplasmic pore. Here, we tested whether charged DEKA-motif residues other than K1237 were also important determinants of a channel's gating properties. Therefore, we constructed the charge-neutralizing mutations D400A, E755A, and K1237A and studied the effects of these mutations on I_{US}. We found that, compared to wild-type $rNa_v1.4$ channels, mutant D400A and K1237A but not E755A channels exhibited enhanced entry into ultra-slow inactivation. Selectivity for Na^+ over K^+, as judged from shifts in reversal potentials, was preserved in D400A, reduced in E755A, and completely lost in K1237A. These data suggest that an electrostatic interaction between the positively charged residue K1237 and the negatively charged residue D400 stabilizes the structure of the pore and thereby prevents I_{US}. Moreover, the interaction between K1237 and E755 appears to provide the basis for selective permeation of Na^+ over K^+.

Voltage-gated Na^+ channels mediate the Na^+ conductance responsible for the rapidly rising phase of the action potential in nerve and muscle cells. Like other voltage-gated ion channels, the main Na^+ channel subunit, α, consists of four homologous domains (DI, DII, DIII, and DIV),[1] each of which is composed of six transmembrane segments (S1−S6). The extracellular loops between S5 and S6 of each domain are proposed to fold back into the membrane to form the outer mouth of the pore and part of the ion-conducting pathway. These loops are called P-loops, and they determine the channel's selectivity (*2*). Specifically, for the Na^+ channel, a restricted number of P-loop amino acid residues are believed to form a narrow constriction of the pore, the so-called selectivity filter (*3*−*5*). These residues are Asp-400 (DI), Glu-755 (DII), Lys-1237 (DIII), and Ala-1529 (DIV; DEKA motif; numbers of the adult rat skeletal muscle Na^+ channel, $rNa_v1.4$). A recent molecular model of the Na^+ channel pore suggests electrostatic interactions between the positively charged DIII residue Lys-1237 with the negatively charged residues Asp-400 (DI) and Glu-755 (DII) to be the key for selective Na^+ conductance and exclusion of other cation species (*6*).

Besides selectivity, interactions of Lys-1237 with Asp-400 and Glu-755 may also determine the structural stability of the pore. Thus, we could recently show that charge-altering mutations at position Lys-1237 (e.g., DIII-K1237E) and at position 1529 (DIV-A1529D) drastically enhanced entry of the channels into an inactivated state from which recovery is very slow (time constants in the order of ~100 s (*1*, *7*)). This state termed "ultra-slow inactivation" (I_{US}) can be elicited by prolonged depolarizations of several 100 s. I_{US} may reflect a collapse of the conduction pathway that involves both the extracellular and the cytoplasmic pore (*1*, *7*, *8*). The fact that I_{US} can hardly be observed in wild-type channels suggests that normally the amino acids at positions 1237 and 1529 stabilize the pore structure and, thus, prevent the pore collapse reflected by I_{US}. Here, we tested possible kinetic effects of altering the charge at the remaining two positions of the DEKA locus, that is, 400 and 755. Furthermore, we explored whether I_{US} can be generated by alteration of only one electronic charge at position 1237 (DIII-K1237A). We found that DI-D400A and DIII-K1237A,

† Supported by Grants P13961-B05 and P17509-B11 provided by the Austrian Science Fund (H.T.) and HL-P01-20592 (H.A.F.).

* To whom correspondence should be addressed. Hannes Todt, Center of Biomolecular Medicine and Pharmacology, Medical University of Vienna, Währingerstrasse 13A, A-1090 Vienna, Austria. Phone, +43-1-4277-64120; fax, +43-1-4277-9641. E-mail, hannes.todt@meduniwien.ac.at.

‡ Medical University of Vienna.

§ The University of Chicago.

|| These authors contributed equally.

[1] Abbreviations: D, domain; I_{US}, ultra-slow inactivation; PCR, polymerase chain reaction.

10.1021/bi0511944 CCC: $30.25
Published on Web 09/27/2005

but not DII-E755A, enhanced entry into I_{US}, suggesting that an electrostatic interaction between Lys-1237 and Asp-400 suffices to stabilize the structure of the pore.

EXPERIMENTAL PROCEDURES

A detailed description of the experimental procedures is given in our previous work (*7*).

Mutagenesis of rNa$_v$1.4. The oligonucleotide-directed point mutations DI-D400A, DII-E755A, and DIII-K1237A were introduced using four-primer PCR. An oligonucleotide containing a mutation was designed with a change in a silent restriction site to allow rapid identification of the mutant. A vector consisting of the rNa$_v$1.4 coding sequence flanked by *Xenopus* globin 5′ and 3′ untranslated regions was provided as a gift by R. Moorman. This was used as the template for mutagenesis, and PCR fragments were isolated and subcloned to this template using directional ligations. Incorporation of the mutation was confirmed by DNA sequencing of the entire polymerized regions. The vector was linearized by *Sal*I digestion and transcribed with SP6 DNA-dependent RNA polymerase using reagents from the mCAP RNA Capping Kit (Stratagene, La Jolla, CA). The rat brain β_1 subunit of the Na^+ channel was also subcloned into pAlterXG and, transcription was prepared from a *Bam*H1-linearized template using SP6 RNA polymerase.

Stage V and VI *Xenopus* oocytes were isolated from female frogs (NASCO, Ft. Atkinson, WI), washed with Ca^{2+}-free solution (90 mM NaCl, 2.5 mM KCl, 1 mM $MgCl_2$, 1 mM $NaHPO_4$, and 5 mM HEPES titrated to pH 7.6 with 1 N NaOH), treated with 2 mg/mL collagenase (Sigma, St. Louis, MO) for 1.5 h, and had their follicular cell layers manually removed. As judged from photometric measurements, approximately 50−100 ng of cRNA was injected into each oocyte with a Drummond microinjector (Broomall, PA). Either native or mutant α subunit cRNA alone or mixed with rat brain β_1 subunit was injected. In some experiments on DI-D400A channels, the injected molar cRNA α/β_1 ratio was 1. Oocytes were incubated at 17 °C for 12 h to 3 days before examination.

Electrophysiological Recordings. Recordings were made in the two-electrode voltage clamp configuration using a TEC 10CD clamp (npi electronic, Tamm, Germany). The clamp amplifier had a series compensation circuit. For accurate adjustment of the experimental temperature (20 ± 0.5 °C), an oocyte bath cooling system (HE 204, Dagan, Minneapolis, MN) was used. Oocytes were placed in recording chambers in which the bath flow rate was about 100 mL/h, and the bath level was adjusted so that the total bath volume was less than 500 μL. Electrodes were filled with 3 M KCl and had resistances of less than 1 MΩ. Using pCLAMP6 (Axon Instruments, Foster City, CA) software, we acquired data at 71.4 kHz after low-pass filtration at 2 kHz (−3 dB). Curve fitting was performed using ORIGIN 5.0 (MicroCal Software, Inc., Northampton, MA). Recordings were made in a bathing solution that consisted of (in millimolar): 90 NaCl, 2.5 KCl, 1 $BaCl_2$, 1 $MgCl_2$, and 5 mM HEPES titrated to pH 7.2 with 1 N NaOH. $BaCl_2$ was used as a replacement for $CaCl_2$ in order to minimize Ca^{2+}-activated Cl^- currents.

Data Evaluation. If not otherwise specified, recovery from I_{US} was tested with the following experimental protocol. From a holding potential of −120 mV, the channels were inactivated by a 300-s depolarizing voltage step. This prepulse duration, rather than longer ones, was normally chosen in order to avoid unacceptably long experimental durations. After the prepulse, the potential was returned to −120 mV, and recovery from inactivation was monitored by repetitive 20-ms test pulses to −20 mV at 20-s intervals. The first test pulse was applied 20 s after the prepulse to allow for recovery from faster forms of inactivation (fast and slow inactivation). The time courses of recovery from I_{US} of normalized peak inward currents were fit with the biexponential function,

$$I_2/I_1 = -A_1 \exp(-t/\tau_1) - A_2 \exp(-t/\tau_2) + C$$

where I_2 is the peak inward Na^+ current of the test pulse during recovery, I_1 is the peak inward Na^+ current of a test pulse under fully available conditions, τ_1 (always constrained to 10 s) and τ_2 (always constrained between 120 and 150 s) are the time constants of distinct components of recovery from inactivation (slow inactivation and I_{US}, respectively), A_1 and A_2 are the respective amplitudes of these time constants, and C is the final level of recovery. A_2 was taken as a measure of the fraction of channels that recovered from I_{US}.

Current−voltage relationships were fit with the function,

$$G_{max}\cdot(V - V_{rev})\cdot(1 - (1/(1 + \exp((V - V_{0.5})/K))))$$

where V is the step potential, G_{max} is the maximum conductance, $V_{0.5}$ is the voltage at which half-maximum activation occurred, V_{rev} is the reversal potential, and K is the slope factor.

Data are expressed as means ± SE. Statistical comparisons were made using two-tailed Student's *t*-tests. A $p < 0.05$ was considered as being significant.

RESULTS

Recovery from I_{US} in Wild-Type and Mutant rNa$_v$1.4 Channels. Figure 1 shows the growth of inward currents through wild-type and various mutant rNa$_v$1.4 channels with subsequent 20-ms test pulses at 20-s intervals. From a holding potential of −120 mV, the channels were first inactivated by a 300-s depolarizing prepulse to either −10 or −50 mV. Recovery from inactivation after returning to −120 mV was monitored through repetitive test pulses to −20 mV (see Experimental Procedures). Figure 2 summarizes the time courses of recovery from inactivation in wild-type and mutant channels. Here, the data points of a series of experiments as shown in Figure 1 were normalized to the respective final current level after full recovery. It can be observed that wild-type and DII-E755A currents quickly recovered from inactivation independent of the prepulse voltage. DI-D400A channels, inactivated by a prepulse to −10 mV, showed a similar quick time course of current recovery (open circles). After −50-mV prepulses, however, the recovery time course of DI-D400A currents was considerably slower (open squares). Finally, recovery of DIII-K1237A currents was dramatically delayed after both −10-mV (open circles) and −50-mV (open squares) prepulses. The data points were fit with two exponentials reflecting two channel populations recovering from slow inactivation and I_{US}, respectively (see Experimental Procedures). The channel

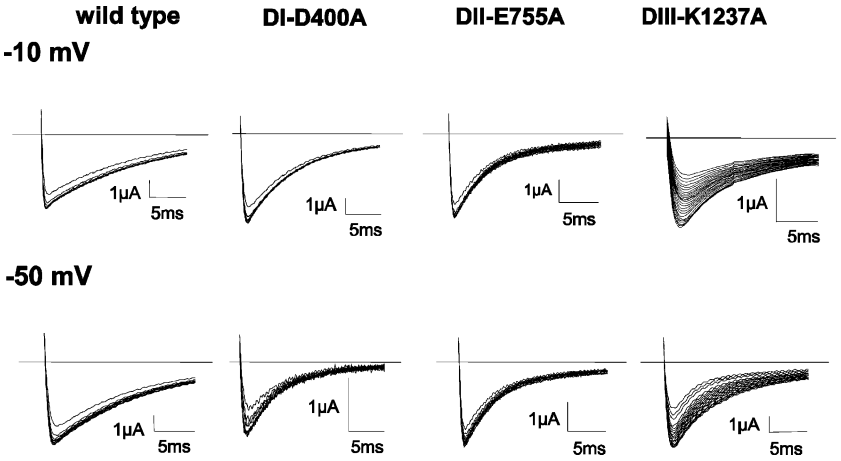

FIGURE 1: Ultraslow inactivation in wild-type and mutant rNa$_v$1.4 channels. Growth of inward currents during recovery from I_{US} in wild-type, DI-D400A, DII-E755A, and DIII-K1237A channels expressed in *Xenopus laevis* oocytes. From a holding potential of −120 mV, the channels were inactivated by a 300-s depolarizing step to −10 mV (upper panel) or −50 mV (lower panel). Thereafter, the potential was returned to −120 mV, and recovery from inactivation was monitored by repetitive 20-ms test pulses to −20 mV at 20-s intervals. The first test pulse was applied 20 s after the prepulse. The horizontal straight lines indicate the zero current levels.

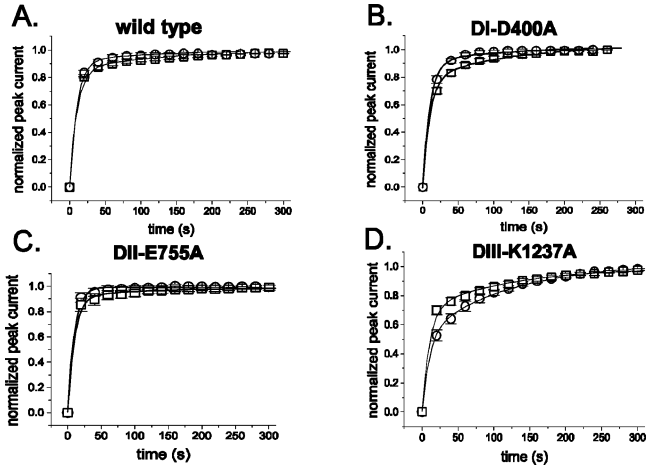

FIGURE 2: Time courses of recovery from ultraslow inactivation. Shown are the time courses of recovery from inactivation of a series of experiments as presented in Figure 1. The data points (means ± SE, *n* values between 3 and 8) were normalized to the respective final current levels after full recovery and fit (solid lines) with two exponentials reflecting two channel populations recovering from slow inactivation and I_{US} (see Experimental Procedures). The data points at zero time were artificially set to zero. For direct comparability, τ_1 and τ_2 were always fixed at 10 and 120 s, respectively. Open circles represent recovery from inactivation after −10 mV prepulses, and open squares represent recovery after −50 mV prepulses.

Table 1: Ultraslow Inactivation in Wild-Type and Mutant rNa$_v$1.4 Channels[a]

rNa$_v$1.4	wild-type	DI-D400A	DII-E755A	DIII-K1237A
−10 mV	0.13 ± 0.02 (4)	0.12 ± 0.03 (6)	0.09 ± 0.02 (5)	0.55 ± 0.05 (4)[b]
−50 mV	0.16 ± 0.02 (4)	0.31 ± 0.04 (6)[b]	0.12 ± 0.01 (3)	0.42 ± 0.05 (8)[b]

[a] Given are the channel fractions (means ± SE (*n*)) recovering from I_{US} after 300-s prepulses to −10 mV and −50 mV. These were obtained from biexponential fits of the recovery time courses as described in Experimental Procedures. For direct comparability, τ_1 and τ_2 were always fixed to 10 and 120 s, respectively, and A_2, the amplitude of τ_2, was taken as a measure of the fraction of channels that recovered from I_{US}. [b] Significantly different from wild-type ($p < 0.05$).

fractions recovering from I_{US}, resulting from this fitting procedure, are given in Table 1. It can be noticed that, compared to wild-type, significantly more channels recovered from I_{US} in mutant DI-D400A after −50-mV prepulses and in mutant DIII-K1237A after both −10-mV and −50-mV prepulses. The largest fraction of channels recovering from I_{US} was found in DIII-K1237A after −10-mV prepulses. These results show that mutations DI-D400A and DIII-K1237A, but not DII-E755A, enhance entry into I_{US}. As for DIV, replacement of alanine by glutamic acid also increases entry into I_{US}, as shown previously (*7*, *8*).

Recovery from I_{US} Following a 1200-s Prepulse in DI-D400A and DIII-K1237A Channels. To test whether a prepulse duration of 300 s was sufficient to drive a maximum fraction of channels into I_{US} and whether I_{US} is an absorbing state in any of our mutants, 1200-s prepulses were applied in a number of experiments. This was done for those mutants which exhibited considerable amounts of I_{US}, DI-D400A, and DIII-K1237A using prepulse voltages which produced maximum I_{US} (−50 mV for DI-D400A and −10 mV for DIII-K1237A). Figure 3 shows that the time course of recovery from I_{US} after a 1200-s prepulse was only modestly delayed compared to that after a 300-s prepulse (Figures 1 and 2) in mutant DI-D400A. Accordingly, the channel fraction recovering from I_{US} after a 1200-s prepulse, 0.42 ± 0.01 ($n = 3$), was only slightly larger than the corresponding fraction after a 300-s prepulse, 0.31 ± 0.04 ($n = 6$). This indicated that development of I_{US} was almost complete after 300-s depolarizations in DI-D400A channels. In contrast, when 1200-s inactivating prepulses instead of 300-s prepulses were applied to mutant DIII-K1237A channels, the channel fraction recovering from I_{US} was dramatically increased (Figure 3) from 0.55 ± 0.05 ($n = 4$) to 0.95 ± 0.02 ($n = 3$). Thus, development of I_{US} was slower in DIII-K1237A than in DI-D400A channels. Moreover, I_{US} is an absorbing state (∼100% occupancy) in mutant DIII-K1237A but not in mutant DI-D400A.

Voltage-Dependence of I_{US} in DI-D400A and DIII-K1237A Channels. The channel fractions recovering from I_{US} were dependent upon the prepulse voltages used in mutant DI-D400A and DIII-K1237A channels (Table 1). Thus, compared to −50-mV prepulses, −10-mV prepulses produced less I_{US} in DI-D400A, whereas more I_{US} in DIII-K1237A channels. To examine the voltage dependencies of I_{US} in these mutants in more detail, 300-s prepulses to voltages

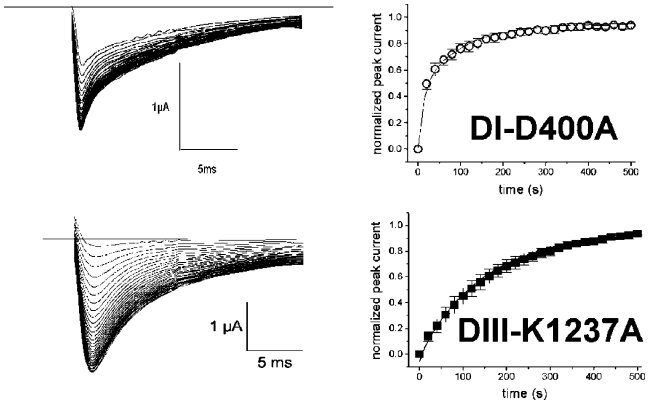

FIGURE 3: Ultraslow inactivation elicited by 1200-s prepulses in mutant rNa$_v$1.4 channels. Growth of inward currents during recovery from I_{US} in DI-D400A and DIII-K1237A channels (left panel). The experimental protocol was identical to that used in Figure 1, except that 1200-s prepulses, instead of 300-s prepulses, were applied. To generate maximum I_{US}, a −50-mV prepulse was applied to DI-D400A channels and a −10-mV prepulse was applied to DIII-K1237A channels. The horizontal straight lines indicate the zero current levels. The right panel summarizes the time courses of recovery from inactivation of a series of experiments as shown in the left panel. The solid lines represent biexponential fits with τ_1 and τ_2 fixed at 10 and 150 s, respectively.

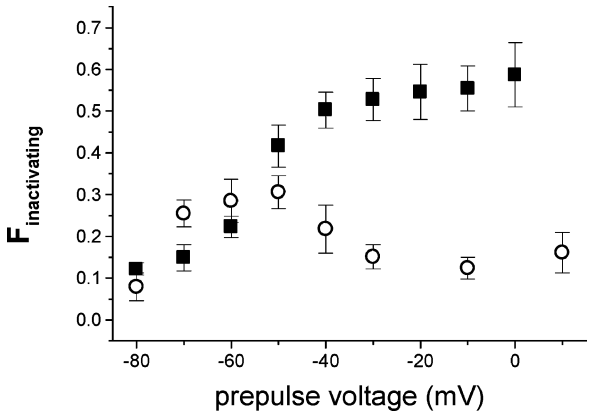

FIGURE 4: Voltage dependence of I_{US} in mutant rNa$_v$1.4 channels. To assess the voltage dependencies of I_{US} in DI-D400A and DIII-K1237A channels, the membrane potential was depolarized from −120 mV to the indicated prepulse voltages for 300 s and the time course of recovery at −120 mV was monitored for each prepulse voltage as described in Figure 1. The time course of recovery from I_{US} was then fit with a biexponential function (see Experimental Procedures) to estimate the fraction of channels recovering from I_{US}. This fraction ($F_{inactivating}$) was plotted as a function of prepulse voltage for mutant DI-D400A (open circles) and mutant DIII-K1237A (filled squares) channels.

between −80 and +10 mV were applied, and recovery from I_{US} was tested. The time course of recovery for each prepulse voltage was then fit with a biexponential function (see Experimental Procedures) to estimate the fraction of channels recovering from I_{US}. This fraction was finally plotted as a function of prepulse voltage in Figure 4. The voltage dependencies of I_{US} showed a striking difference between mutant DI-D400A and DIII-K1237A channels. It was U-shaped in DI-D400A (open circles) with a local maximum at −50 mV, whereas S-shaped in DIII-K1237A (filled squares) channels.

Effects of Coexpression of the β_1-Subunit on I_{US} in DI-D400A Channels. In the mutant DIV-A1529D, which also exhibited a U-shaped voltage dependence of I_{US}, we have previously found that coexpression of the Na^+ channel β_1-subunit inhibited entry of channels into I_{US} (*8*). In this study, we suggested that binding of the fast inactivation gate to its cytoplasmic receptor inhibits I_{US}, which may finally result in a U-shaped voltage dependence of I_{US} (see Discussion). The β_1-subunit is known to stabilize fast inactivation (for example, see refs *9*, *10*) and may thereby inhibit I_{US}. Because DI-D400A channels also showed a U-shaped voltage dependence of I_{US}, we reasoned that the β_1-subunit may inhibit entry into I_{US} also in this mutant. To test this, we coexpressed the rat brain β_1-subunit with DI-D400A α-subunits and studied their I_{US} properties. Figure 5 shows the growth of inward currents through DI-D400A + β_1 channels with subsequent test pulses at 20-s intervals (upper panel). Compared to DI-D400A α-only channels (Figure 1), the current decay following channel activation of DI-D400A + β_1 channels was dramatically accelerated. This confirmed functional association of β_1-subunits with DI-D400A α-subunits. Moreover, the channel fraction recovering from I_{US} in DI-D400A + β_1 channels after a 300-s prepulse to −50 mV, 0.18 ± 0.02 (n = 5), was significantly reduced compared to the corresponding fraction of DI-D400A α-only channels, 0.31 ± 0.04 (n = 6). Thus, coexpression of the β_1-subunit inhibited entry into I_{US} also in DI-D400A channels.

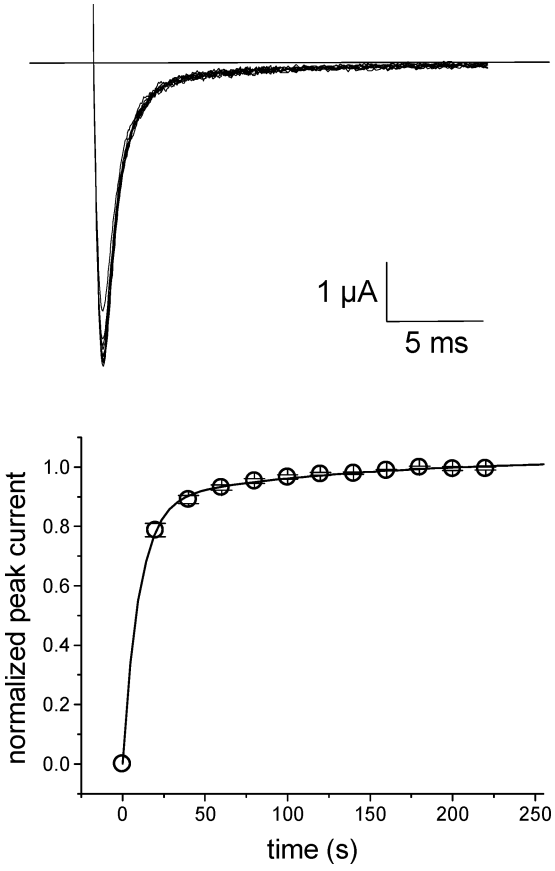

FIGURE 5: Ultraslow inactivation in mutant DI-D400A + β_1 channels. Growth of inward currents during recovery from I_{US} (upper panel). DI-D400A α-subunits were coexpressed with rat brain β_1-subunits in *Xenopus laevis* oocytes (molar cRNA α_1/β ratio = 1). The experimental protocol was identical to that used in Figure 1. A 300-s prepulse to −50 mV was applied. The horizontal straight line indicates the zero current level. The lower panel summarizes the time courses of recovery from inactivation of a series of experiments as shown in the upper panel. The solid line represents a biexponential fit with τ_1 and τ_2 fixed at 10 and 120 s, respectively.

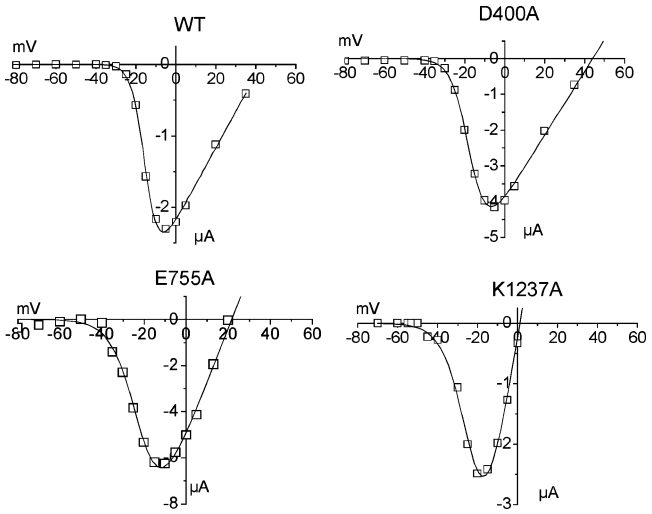

FIGURE 6: Current−voltage relationships of wild-type and mutant $rNa_v1.4$ channels. From a holding potential of −120 mV, 20-ms test pulses to voltages between −80 and +40 mV were applied to activate the channels. The peaks of the elicited inward currents were then plotted against the test pulse voltage to obtain current−voltage relationships, typical examples of which are shown for wild-type, DI-D400A, DII-E755A, and DIII-K1237A channels. The solid lines represent fits using the function given in Experimental Procedures.

Table 2: Reversal Potentials of Wild-Type and Mutant $rNa_v1.4$ Channels[a]

$rNa_v1.4$	wild-type	DI-D400A	DII-E755A	DIII-K1237A
V_{rev}	43.7 ± 1.9 (6)	43.1 ± 1.1 (4)	33.6 ± 2.9 (5)[b]	−1.4 ± 1.1 (6)[b]

[a] The reversal potentials (V_{rev} values, means ± SE (n); mV) were determined by fitting current−voltage relationships using the fitting procedure described in Experimental Procedures. [b] Significantly different from wild-type ($p < 0.05$).

Reversal Potentials of Wild-Type and Mutant $rNa_v1.4$ Channels. To test the effects of mutations DI-D400A, DII-E755A, and DIII-K1237A on channel selectivity, we compared the current−voltage relationships of mutant channels with those of wild-type channels. From a holding potential of −120 mV, 20-ms test pulses to voltages between −80 and +40 mV were applied to activate the channels. The peaks of the elicited inward currents were then plotted against the test pulse voltage to obtain current−voltage relationships, typical examples of which are shown in Figure 6. It can be observed that the voltages at which the Na^+ currents reversed their direction (reversal potentials, V_{rev} values) significantly differed between mutant and wild-type channels. Whereas DI-D400A channels had a very similar V_{rev} as wild-type channels, the V_{rev} values of DII-E755A and DIII-K1237A channels were significantly shifted toward more negative potentials (Table 2). This shift was moderate in DII-E755A channels and dramatic in DIII-K1237A channels, suggesting a weak and a strong effect of the respective mutation on Na^+ channel selectivity.

DISCUSSION

The Outer Vestibule Is a Highly Flexible Structure. A number of studies have demonstrated that the P-loops of voltage-gated Na^+ channels are highly flexible structures (*11*, *12*). This high degree of flexibility most likely results from the fact that these loops fold back into the pore lumen surrounded by the S6 segments and may have only weak contacts with the α-helices of the S6 segments. Recent molecular dynamics simulations suggest that the fluctuating nature of the pore may be essential for the process of selectivity of permeation (*13*−*15*). Nevertheless, some degree of stabilization of the delicate structure of the outer vestibule has to be present. In potassium channels, the three-dimensional structure of the outer vestibule is stabilized by intra- and intersegment H-bonds (*16*). Analogously, in voltage-gated Na^+ channels, stabilization may be provided by interactions between residues of different P-loops (*11*, *17*). Obviously, such interactions are most important at the level where the P-loops converge to form the selectivity filter given by the DEKA-motif. Experimentally, interactions between P-loop residues have been demonstrated by systematically introducing pairs of cysteines throughout the pore-lining segments. Thus, the mutant DI-Y401C ($rNa_v1.4$) spontaneously formed a disulfide bond when paired with DII-E758C, suggesting that the pore loop residues of DI and DII are in close proximity (*18*). Furthermore, DI-Y401C paired with DIV-G1530C created a high affinity binding site for cadmium (*18*). As for the DEKA-motif, an interaction among its residues is suggested by the fact that the mutant DEAA is permeable to larger organic cations than the mutants DAAA, AEAA, and AAAA (*17*). In DEAA, electrostatic repulsion may act to widen the pore to a greater diameter than in mutants with only one charged residue or in AAAA. On the other hand, in DEKA, the positively charged DIII-K1237 may partially cancel the repulsive action between negatively charged DI-D400 and DII-E755, causing the aperture to constrict (*17*). Taking these data into account, Lipkind and Fozzard proposed a model of ion permeation through the selectivity filter: the DIII-K1237 side chain is proposed to be in immediate contact with DII-E755 with formation of hydrogen bond or salt bridge, while DI-D400 could interact with DIII-K1237 through a water bridge (*6*). During permeation, the Na^+ ion may displace the ammonium group of DIII-K1237 from its interaction with the carboxyls. Clearly, mutations in this region of delicately balanced interactions may not only result in altered permeation properties but also in structural changes of the outer vestibule, which, in turn, may alter the gating properties of the channel.

Mutations in the Outer Vestibule Alter Channel Gating. We have previously reported that charge-altering mutations (DIII-K1237E, DIII-K1237S), but not the charge-preserving mutation DIII-K1237R, at position Lys-1237 in DIII (*1*), drastically enhanced entry of $rNa_v1.4$ channels into an inactivated state with abnormally slow recovery kinetics, I_{US}. This indicated that the positive charge of Lys-1237 is essential for preventing the conformational change reflected by I_{US}. The present study further confirms this view by adding DIII-K1237A to the list of charge-altering Lys-1237 mutations which enhance I_{US}. Interestingly, the notion that a positively charged amino acid in the selectivity filter of Na^+ channels serves the purpose to stabilize the structure is also supported by recent mutagenesis studies in the bacterial Na^+ channel from *Bacillus halodurans* (NaChBac). Here, the only positive charge in the NaChBac pore loop is distal to the presumed selectivity filter (R199). Neutralization (R199A) or replacement with a negatively charged amino acid (R199D) yields a channel that is either nonconducting or too purely conducting to yield measurable current (*19*).

Besides DIII-K1237, the DEKA-motif residue of DIV, DIV-A1529, may also be important for preserving the pore structure. Accordingly, mutation DIV-A1529D was shown to enhance entry into I_{US} (*7*, *8*). It is possible that this mutation electrostatically destabilizes and weakens the interaction between DIII-K1237 and DI-D400 which normally stabilizes the pore.

The main new finding of the present study is the demonstration that mutation DI-D400A of the DI P-loop, but not DII-E755A of the DII P-loop, destabilizes the pore structure as represented by a higher likelihood to enter into I_{US}. Thus, enhanced I_{US}, compared to wild-type channels, can be generated by charge-altering mutations not only at position 1237 and 1529 (*7*, *8*) but also at position 400. The only exception appears to be mutation DII-E755A which had no effect on I_{US}. In the following section, we develop a mechanistic model that may account for the experimental data.

Proposed Mechanism of I_{US}. Recently, we demonstrated that the local anesthetic agent lidocaine inhibits I_{US}, produced by the mutation DIII-K1237E, by acting as a foot-in-the-door of the inner vestibule of the channel (*20*). This action of lidocaine occurs by binding to residue F1579 located approximately in the middle of the DIV-S6 segment. We proposed that I_{US} represents a conformational change of the DIV-S6 segment resulting in a long-lived nonconducting state of the channel ("collapse of the inner vestibule"). Since the mutation which generated I_{US} (K1237E) is located in the outer vestibule of the channel, the conformational change produced by the mutation DIII-K1237E must somehow be transmitted to the DIV-S6 segment. This transmission must occur during inactivation, since I_{US} can only be induced by prolonged depolarizations. Furthermore, the structural change imposed by charge-altering mutations of residue DIII-K1237 in the outer vestibule is most likely associated with a widening of this region, as the DIII-K1237A channel becomes permeable to a number of large cations (*17*, *21*). Molecular modeling places DIII-K1237 close to residue I1575 of the α-helix of DIV-S6 (*6*). The mutation DIII-K1237E may induce a lateral movement of residue DIII-E1237 by electrostatic repulsion from the neighboring residues DI-D400 and DII-E755. During inactivation, this lateral displacement of DIII-E1237 may elicit a conformational change of the DIV-S6 segment, perhaps via interaction with residue I1575, which ultimately results in entry into the long-lived inactivated state represented by I_{US}. We recently presented evidence for such an interaction: in the background of the mutation DIII-K1237E, the additional mutation I1575E abolished I_{US}. In this double mutant, the electrostatic repulsion between DIII-E1237 and DIV-E1575 may have prevented the interaction between the DIII P-loop and the DIV-S6 segment that gives rise to I_{US} (*22*). Thus, the DIV-S6 segment may have a fundamental role in the generation of long-lived inactivated states. As mentioned above, such a role for the DIV-S6 segment in slow inactivation was suggested by the fact that binding of lidocaine to F1579 strongly modulated I_{US}. Apart from this finding, a number of mutations in S6 segments have been reported to affect slow-inactivated states (*23*−*26*). Furthermore, in $K_V1.4$ channels, slow inactivation is associated with a decrease in intracellular aqueous pore volume (*27*), again emphasizing a significant role of the inner vestibule (which is considered to be lined by the S6 segments) in slow inactivation gating. Furthermore, the unique functional role of the gating apparatus of DIV in inactivation gating also appears to apply to the voltage sensors in this domain. Thus, the voltage sensors in domains III and IV appear to be responsible for the voltage-sensitive conformational changes linked to inactivation (*28*, *29*).

Therefore, we propose that I_{US} is generated by an abnormal movement of the DIV-S6 helix during inactivation. This abnormal movement may result from an interaction of the DIII P-loop with the adjacent DIV-S6 helix caused by an lateral movement of the DIII P-loop as a consequence of the DIII-K1237E mutation (Figure 7B). A similar effect is likely to be the cause for I_{US} produced by DIII-K1237A, as shown in this study.

How can the effect of the mutations in DI, DII, and DIV P-loops be reconciled with this model? Molecular modeling places the DIV-S6 segment in close contact not only to the DIII P-loop but also to the DIV P-loop (*6*). Thus, abnormal movements of the DIV P-loop, as perhaps generated by the mutation DIV-A1529D, may be transmitted to DIV-S6, offering an explanation for the substantial propensity of DIV-A1529D channels to enter into I_{US} (Figure 7C).

In the case of the mutation DI-D400A, it can be presumed that this mutation increases the flexibility of the DI P-loop. This motion could be transmitted to the DV-S6-segment via the DIV P-loop, which itself has been shown to be extraordinarily flexible (*11*; Figure 7D). As mentioned above, DI-Y401C paired with DIV-G1530C created a high affinity binding site for cadmium (*18*), indicating that the P-loops of DI and DIV are in close contact with each other. Thus, it is not unreasonable to assume that conformational changes in the DI P-loop, as perhaps induced by the mutation DI-D400A, may be transmitted to the DIV P-loop. Similarly, the DII-E755A mutation may be expected to increase the mobility of the DII P-loop. However, this increase in motion may not easily be transmitted to the DIV-S6 segment because the DIII-K1237 next to DIV-S6 still can form an interaction with DII-E755 thus restricting the mobility of this residue, which, in turn, may protect the DIV-S6 segment from the increased mobility of the DII P-loop (Figure 7E).

Impact of the DEKA Mutations on Selectivity. The reversal potentials shown in Table 2 indicate that selectivity of permeation is unchanged in DI-D400A, reduced in DII-E755A, and abolished in DIII-K1237A. These data are consistent with previous studies (*17*, *30*). Hence, DI-D400A produces I_{US} but does not interfere with selectivity of permeation, whereas DII-E755A has no effect on I_{US} but reduces selectivity of permeation. It is hard to speculate on the mechanistic basis of this divergent effects of the mutations on selectivity and gating. Perhaps some degree of flexibility of the P-loop structure has to be present for the proper function of the selectivity filter (*13*−*15*). In the wild-type channel, DIII-K1237 is proposed to predominantly interact with DII-E755 (*6*). This interaction is lost in DII-E755A and is probably replaced by a new interaction between DIII-K1237 and DI-400 (*6*). It is possible that the interaction of DIII-K1237 and DI-D400 in DII-E755A reduces the flexibility of the pore, which, on one hand, protects from entry into I_{US} but, on the other hand, reduces the selectivity of the channel. In DI-D400A, the "physiologic" interaction between DIII-K1237 and DII-E755

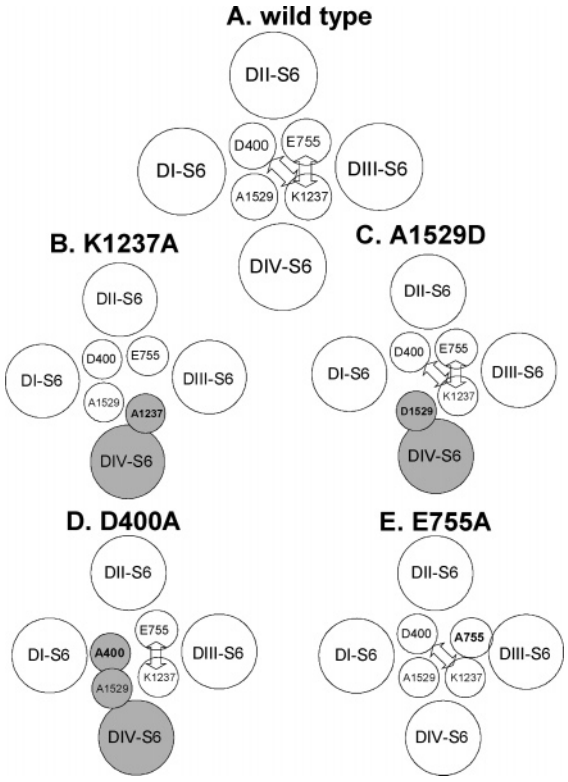

FIGURE 7: Cartoon of the outer vestibule of the voltage-gated Na^+ channel. Top view, showing the S6 segments of domains I−IV and the amino acids DI-D400, DII-E755, DIII-K1237, and DIV-K1237, which are considered to form the selectivity filter. The domains are arranged clockwise, as supported by studies of the interactions of the guanidinium toxins and μ-conotoxin (*40*−*42*). The close relationship between S6 segments and P-loop residues corresponds to a model using the KcsA crystal structure as framework for a molecular model of the pore of the voltage-gated Na^+ channel (*6*). Regions of the channel which interact with each other thereby producing I_{US} are indicated by shading. Possible electrostatic interactions between DEKA residues are indicated by arrows. (A) Wild-type, electrostatic interactions between residues DIII-K1237, DI-D400, and DII-E755 stabilize the structure of the selectivity filter. (B) Mutation DIII-K1237A, the electrostatic interactions between residues DIII-K1237, DI-D400, and DII-E755 are lost, resulting in a displacement of the DIII P-loop. This displacement produces an interaction between the DIII P-loop and the DIV-S6 segment, resulting in I_{US}. (C) Mutation DIV-A1529D, the negative charge in DIV produces an electrostatic repulsion between the P-loops of DIV and DI resulting in an interaction of DIV P-loop and DIV-S6, giving rise to I_{US}. (D) Mutation DI-D400A, the electrostatic interaction between DI-D400 and DIII-K1237 is lost, resulting in a displacement of the DI P-loop which produces an interaction between the P-loops of DI and DIV, which, in turn, gives rise to an interaction between the DIV P-loop and DIV-S6. This interaction between the DIV P-loop and DIV-S6 causes the mutant channel to enter into I_{US} upon prolonged depolarizations. (E) Mutation DII-E755A, the electrostatic interaction between DII-E755 and DIII-K1237 is lost. However, DI-D400 still interacts with DIII-K1237 thereby stabilizing the structure of the selectivity filter. Hence, this mutations does not give rise to I_{US}.

remains unchanged, which may explain why the selectivity in this mutant is not affected.

Different Voltage Dependencies of I_{US} in DI-D400A and DIII-K1237A Channels. We have previously shown that the time constants of recovery from I_{US} were similar in channels which contained charge-altering mutations in the DEKA motif residues of DIII and DIV. In contrast, the voltage dependencies of I_{US} showed a striking difference: it was S-shaped in DIII-K1237E and DIII−K1237S channels (*1*), but U-shaped in DIV-A1529D channels (*7*, *8*). In Hilber et al. (*8*), we found that stabilization of the fast-inactivated state (e.g., by coexpression of the Na^+ channel β_1-subunit) inhibited entry into I_{US}. We concluded that binding of the fast inactivation gate (IFM motif in the DIII-DIV linker; *31*, *32*) to its cytoplasmic receptor might stabilize the channel pore and thereby prevent I_{US}. The probability of channels to undergo fast inactivation increases at more positive potentials, and thus, inhibition of I_{US} by fast inactivation (especially at strongly depolarized potentials > -50 mV) may contribute to produce a U-shaped voltage dependence in DIV-A1529D channels. This could indeed be confirmed in experiments where we disrupted fast inactivation by the additional mutations I1303Q/F1304Q/M1305Q in DIV-A1529D channels and observed enhanced I_{US} at strongly depolarized potentials (*8*).

In the present study, we explored the voltage dependencies of I_{US} in two new mutants which exhibited considerable amounts of I_{US}, DIII-K1237A and DI-D400A. As expected, DIII-K1237A channels showed an S-shaped voltage dependence very similar to the voltage dependencies of DIII-K1237E and DIII-K1237S channels (*1*). In contrast, DI-D400A channels had a U-shaped voltage dependence with a local maximum at -50 mV, thus, comparable with that previously observed in DIV-A1529D channels (*7*, *8*). The reason for the striking difference in the voltage dependencies of I_{US} between DIII-Lys1237 mutations and mutations DIV-A1529D as well as DI-D400A is unknown and can only be speculated about. It is remarkable that the DIII-Lys1237 mutations drive a large channel fraction into I_{US} ($\sim$1 after 1200-s depolarizing prepulses; this study; *20*), whereas the respective fractions in DIV-A1529D ($\sim$0.6; *7*) and DI-D400A ($\sim$0.4; this study) are considerably reduced. Thus, it seems that the DIII-Lys1237 mutations more severely destabilize the pore structure than mutations DIV-A1529D and DI-D400A, and this may finally result in basically different voltage dependencies of I_{US}. It is possible that binding of the fast inactivation gate to its cytoplasmic receptor stabilizes the pore structure and inhibits I_{US} in mutations DIV-A1529D (*8*) and DI-D400A (this study) which, compared to the DIII-Lys1237 mutations, less severely destabilize the pore. This may result in a U-shaped voltage dependence of I_{US} (see above). On the other hand, binding of the fast inactivation gate to its receptor in the DIII-Lys-1237 mutations, which more severely destabilize the pore, may not sufficiently stabilize in order to significantly prevent I_{US}. This may result in a "normal" S-shaped voltage dependence of I_{US}.

If these considerations are true, stabilization of the fast-inactivated state should have no effect on I_{US} in the DIII-Lys-1237 mutations, whereas it inhibits I_{US} in DIV-A1529D and DI-D400A. Accordingly, no considerable effect of β_1-subunit coexpression (which stabilizes the fast-inactivated state; for example, see refs *9*, *10*) on I_{US} was found in DIII-K1237E (*1*). In contrast, β_1-subunit coexpression significantly inhibited I_{US} in DIV-A1529D (*8*) and DI-D400A (this study). These findings are in line with the idea that a U-shaped voltage dependence of I_{US} is observed in mutations which only modestly destabilize the pore structure. Mutations more severely destabilizing the pore seem to produce an S-shaped voltage dependence of I_{US}.

Apart from voltage-gated Na^+ channels, U-shaped voltage dependence of inactivation has also been observed in delayed rectifier K^+ channels and in N-type calcium channels (*33*−*35*). In these channels, the occupancy of slow-inactivated states is maximal at intermediate potentials, because at these potentials specific closed states are populated. These "partially activated" closed states are connected to slow-inactivated states, which may be populated if the membrane potential is held at intermediate values long enough to allow entry into slow inactivation (*33*−*35*). Activation of ion channels is considered to arise from an opening of the inner pore of the channel by a concerted movement of the S6 segments (*36*). Thus, closed states on the way to the final open state most likely are associated with certain conformations of the S6 segments before the "bundle crossing" is opened. Interestingly, in K^+ channels, U-type inactivation is modulated by mutations of cytoplasmic parts of the channel, either in the S6 segments or the T1 domain (*37*, *38*). These data are in good agreement with our previous finding that in $Na_v1.4$ lidocaine interferes with ultraslow inactivation by acting as a foot-in-the-door of the inner vestibule (*20*) and strongly support the notion that some types of slow inactivation result from a conformational change at the inner vestibule of the channel.

The conclusions of the present study are based on the examination of the kinetic effects of charge-altering mutations. Therefore, possible molecular interactions revealed by these mutations can be considered to be of electrostatic nature. However, some functions of the outer vestibule are not limited to electrostatic interactions but may require the identity of certain amino acids at defined positions. For example, it has been demonstrated that the exclusion of Ca^{2+} ions by the 1237 site in the DEKA-motif is mainly based on electrostatic interactions, whereas the exclusion of K^+ requires the identity of a lysine at position 1237. Thus, the conservative mutation K1237R is not permeable to Ca^{2+} but readily conducts K^+ ions (*30*). On the other hand, the mutation K1237R does not increase the likelihood of entry into I_{US} (*1*). By contrast, the charge-altering mutations K1237E, K1237S (*1*), K1237C (*39*), and K1237A (this study) all render channels susceptible to I_{US}. This suggests that the propensity to enter I_{US} is mainly determined by electrostatic interactions.

In summary, the presented data and data from previous studies suggest that mutations of DEKA residues from all domains except DII enhance entry into I_{US}. This effect most likely occurs by interaction of the P-loops with the DIV-S6 segment, ultimately resulting in a conformational change of the inner vestibule, which is reflected by entry into the long-lived inactivated state I_{US}. Further studies will be necessary to confirm this proposed mechanism.

ACKNOWLEDGMENT

We thank Mr. Anton Karel and Mrs. Eva Weisz for technical assistance.

REFERENCES

1. Todt, H., Dudley, S. C. J., Kyle, J. W., French, R. J., and Fozzard, H. A. (1999) Ultra-slow inactivation in μ1 Na^+ channels is produced by a structural rearrangement of the outer vestibule, *Biophys. J. 76*, 1335−1345.
2. Guy, H. R., and Conti, F. (1990) Pursuing the structure and function of voltage-gated channels, *Trends Neurosci. 13*, 201−206.
3. Terlau, H., Heinemann, S. H., Stühmer, W., Pusch, M., Conti, F., Imoto, K., and Numa, S. (1991) Mapping the site of block by tetrodotoxin and saxitoxin of sodium channel II, *FEBS Lett. 293*, 93−96.
4. Heinemann, S. H., Terlau, H., Stühmer, W., Imoto, K., and Numa, S. (1992) Calcium channel characteristics conferred on the sodium channel by single mutations, *Nature 356*, 441−443.
5. Lipkind, G. M., and Fozzard, H. A. (1994) A structural model of the tetrodotoxin and saxitoxin binding site of the Na^+ channel, *Biophys. J. 66*, 1−13.
6. Lipkind, G. M., and Fozzard, H. A. (2000) KcsA crystal structure as framework for a molecular model of the Na^+ channel pore, *Biochemistry 39*, 8161−8170.
7. Hilber, K., Sandtner, W., Kudlacek, O., Glaaser, I. W., Weisz, E., Kyle, J. W., French, R. J., Fozzard, H. A., Dudley, S. C., and Todt, H. (2001) The selectivity filter of the voltage-gated sodium channel is involved in channel activation, *J. Biol. Chem. 276*, 27831−27839.
8. Hilber, K., Sandtner, W., Kudlacek, O., Schreiner, B., Glaaser, I., Schutz, W., Fozzard, H. A., Dudley, S. C., and Todt, H. (2002) Interaction between fast and ultra-slow inactivation in the voltage-gated sodium channel. Does the inactivation gate stabilize the channel structure?, *J. Biol. Chem. 277*, 37105−37115.
9. Schreibmayer, W., Wallner, M., and Lotan, I. (1994) Mechanism of modulation of single sodium channels from skeletal muscle by the beta 1-subunit from rat brain, *Pfluegers Arch. 426*, 360−362.
10. Balser, J. R., Nuss, H. B., Romashko, D. N., Marban, E., and Tomaselli, G. F. (1996) Functional consequences of lidocaine binding to slow-inactivated sodium channels, *J. Gen. Physiol. 107*, 643−658.
11. Benitah, J. P., Ranjan, R., Yamagishi, T., Janecki, M., Tomaselli, G. F., and Marban, E. (1997) Molecular motions within the pore of voltage-dependent sodium channels, *Biophys. J. 73*, 603−613.
12. Benitah, J. P., Chen, Z., Balser, J. R., Tomaselli, G. F., and Marban, E. (1999) Molecular dynamics of the sodium channel pore vary with gating: interactions between P-segment motions and inactivation, *J. Neurosci. 19*, 1577−1585.
13. Noskov, S. Y., Berneche, S., and Roux, B. (2004) Control of ion selectivity in potassium channels by electrostatic and dynamic properties of carbonyl ligands, *Nature 431*, 830−834.
14. Allen, T. W., Andersen, O. S., and Roux, B. (2004) On the importance of atomic fluctuations, protein flexibility, and solvent in ion Permeation, *J. Gen. Physiol. 124*, 679−690.
15. Kurata, Y., Sato, R., Hisatome, I., and Imanishi, S. (1999) Mechanisms of cation permeation in cardiac sodium channel: description by dynamic pore model, *Biophys. J. 77*, 1885−1904.
16. Doyle, D. A., Morais, C. J., Pfuetzner, R. A., Kuo, A., Gulbis, J. M., Cohen, S. L., Chait, B. T., and MacKinnon, R. (1998) The structure of the potassium channel: molecular basis of K^+ conduction and selectivity, *Science 280*, 69−77.
17. Sun, Y., Favre, I., Schild, L., and Moczydlowski, E. (1997) On the structural basis for size-selective permeation of organic cations through the voltage-gated sodium channel: effect of alanine mutations at the DEKA locus on selectivity, inhibition by Ca^{2+} and H^+, and molecular sieving, *J. Gen. Physiol. 110*, 693−715.
18. Benitah, J. P., Tomaselli, G. F., and Marban, E. (1996) Adjacent pore-lining residues within sodium channels identified by paired cysteine mutagenesis, *Proc. Natl. Acad. Sci. U.S.A. 93*, 7392−7396.
19. Yue, L., Navarro, B., Ren, D., Ramos, A., and Clapham, D. E. (2002) The cation selectivity filter of the bacterial sodium channel, NaChBac, *J. Gen. Physiol. 120*, 845−853.
20. Sandtner, W., Szendroedi, J., Zarrabi, T., Zebedin, E., Hilber, K., Glaaser, I., Fozzard, H. A., Dudley, S. C., and Todt, H. (2004) Lidocaine: a foot in the door of the inner vestibule prevents ultra-slow inactivation of a voltage-gated sodium channel, *Mol. Pharmacol. 66*, 648−657.
21. Sun, W., Barchi, R. L., and Cohen, S. A. (1995) Probing sodium channel cytoplasmic domain structure. Evidence for the interaction of the rSkM1 amino and carboxyl termini, *J. Biol. Chem. 270*, 22271−22276.

22. Zarrabi, T., Sandtner, W., Szendroedi, J., Zebedin, E., Fozzard, H. A., Hilber, K., and Todt, H. (2005) The structure of the pore of the voltage-gated sodium channel is stabilized by an interaction between the selectivity filter and the DIV-S6 segment, *Biophys. J. 88*, 94a.
23. Wang, S. Y., and Wang, G. K. (1997) A mutation in segment I-S6 alters slow inactivation of sodium channels, *Biophys. J. 72*, 1633−1640.
24. Takahashi, M. P., and Cannon, S. C. (1999) Enhanced slow inactivation by V445M: a sodium channel mutation associated with myotonia, *Biophys. J. 76*, 861−868.
25. O'Reilly, J. P., Wang, S. Y., and Wang, G. K. (2000) A point mutation in domain 4-segment 6 of the skeletal muscle sodium channel produces an atypical inactivation state, *Biophys. J. 78*, 773−784.
26. O'Reilly, J. P., Wang, S. Y., and Wang, G. K. (2001) Residue-specific effects on slow inactivation at V787 in D2-S6 of Nav 1.4 sodium channels, *Biophys. J. 81*, 2100−2111.
27. Jiang, X., Bett, G. C., Li, X., Bondarenko, V. E., and Rasmusson, R. L. (2003) C-type inactivation involves a significant decrease in the intracellular aqueous pore volume of Kv1.4 K^+ channels expressed in *Xenopus* oocytes, *J. Physiol. 549*, 683−695.
28. Cha, A., Ruben, P. C., George, A. L. J., Fujimoto, E., and Bezanilla, F. (1999) Voltage sensors in domains III and IV, but not I and II, are immobilized by Na^+ channel fast inactivation, *Neuron 22*, 73−87.
29. Sheets, M. F., Kyle, J. W., Kallen, R. G., and Hanck, D. A. (1999) The Na channel voltage sensor associated with inactivation is localized to the external charged residues of domain IV, S4, *Biophys. J. 77*, 747−757.
30. Favre, I., Moczydlowski, E., and Schild, L. (1996) On the structural basis for ionic selectivity among Na^+, K^+, and Ca^{2+} in the voltage-gated sodium channel, *Biophys. J. 71*, 3110−3125.
31. West, J. W., Patton, D. E., Scheuer, T., Wang, Y., Goldin, A. L., and Catterall, W. A. (1992) A cluster of hydrophobic amino acid residues required for fast Na^+-channel inactivation, *Proc. Natl. Acad. Sci. U.S.A. 89*, 10910−10914.
32. Patton, D. E., West, J. W., Catterall, W. A., and Goldin, A. L. (1992) Amino acid residues required for fast Na^+-channel inactivation: charge neutralizations and deletions in the III−IV linker, *Proc. Natl. Acad. Sci. U.S.A. 89*, 10905−10909.
33. Klemic, K. G., Shieh, C. C., Kirsch, G. E., and Jones, S. W. (1998) Inactivation of Kv2.1 potassium channels, *Biophys. J. 74*, 1779−1789.
34. Patil, P. G., Brody, D. L., and Yue, D. T. (1998) Preferential closed-state inactivation of neuronal calcium channels, *Neuron 20*, 1027−1038.
35. Jones, L. P., DeMaria, C. D., and Yue, D. T. (1999) N-type calcium channel inactivation probed by gating-current analysis, *Biophys. J. 76*, 2530−2552.
36. Perozo, E., Cortes, D. M., and Cuello, L. G. (1999) Structural rearrangements underlying K^+-channel activation gating, *Science 285*, 73−78.
37. Kurata, H. T., Soon, G. S., Eldstrom, J. R., Lu, G. W., Steele, D. F., and Fedida, D. (2002) Amino-terminal determinants of U-type inactivation of voltage-gated K^+ channels, *J. Biol. Chem. 277*, 29045−29053.
38. Kurata, H. T., Soon, G. S., and Fedida, D. (2001) Altered state dependence of c-type inactivation in the long and short forms of human Kv1.5, *J. Gen. Physiol. 118*, 315−332.
39. Sandtner, W., Szendroedi, J., Hilber, K., Kudlacek, O., Zebedin, E., French, R. J., Fozzard, H. A., Dudley, S. C., and Todt, H. (2003) A constriction of the selectivity filter produces ultra-slow inactivation in voltage-gated Na^+ channels, *Biophys. J. 84*, 67a.
40. Dudley, S. C., Chang, N., Hall, J., Lipkind, G., Fozzard, H. A., and French, R. J. (2000) μ-Conotoxin GIIIA interactions with the voltage-gated Na^+ channel predict a clockwise arrangement of the domains, *J. Gen. Physiol. 116*, 679−690.
41. Li, R. A., Ennis, I. I., French, R. J., Dudley, S. C., Tomaselli, G. F., and Marban, E. (2001) Clockwise domain arrangement of the sodium channel revealed by beta-conotoxin (GIIIA) docking orientation, *J. Biol. Chem. 276*, 11072−11077.
42. Penzotti, J. L., Fozzard, H. A., Lipkind, G. M., and Dudley, S. C. J. (1998) Differences in saxitoxin and tetrodotoxin binding revealed by mutagenesis of the Na^+ channel outer vestibule, *Biophys. J. 75*, 2647−2657.

BI0511944